engineering proceedings

MDPI

Proceeding Paper

Impact of Electrical Noise on the Accuracy of Resistive Sensor Measurements Using Sensor-to-Microcontroller Direct Interface †

Marco Grossi * and Martin Omaña

Department of Electrical Energy and Information Engineering "Guglielmo Marconi" (DEI), University of Bologna, 40136 Bologna, Italy; martin.omana@unibo.it
* Correspondence: marco.grossi8@unibo.it; Tel.: +39-0512093038
† Presented at the 12th International Electronic Conference on Sensors and Applications (ECSA-12), 12–14 November 2025; Available online: https://sciforum.net/event/ECSA-12.

Abstract

Wireless sensor networks (WSNs) implemented in the paradigm of the Internet of Things (IoT) are characterized by a large number of distributed sensor nodes that make measurements in-the-field and communicate with other sensor nodes and servers in the cloud by means of wireless technology. Sensor-to-microcontroller direct interface (SMDI) is a technique used for the measurement of resistive sensors without the use of an ADC. In SMDI based measurements, the sensor is directly interfaced with the digital input-output pins of the general purpose input output (GPIO) interface of microcontrollers and FPGAs. Compared with the measurements per-formed with an ADC, SMDI is characterized by lower cost and lower power consumption. In this paper, the impact of noise on the accuracy of resistive sensor measurements using SMDI is investigated. The study was carried out by LTSpice electrical level simulations and validated by preliminary experimental measurements, where a set of resistances in the range from 100 Ω to 10 kΩ were measured by SMDI under different levels of noise. For each operative condition, the simulations were also carried out in the case of measurements performed with a 12-bit ADC and the achieved accuracy for the measured resistances was compared with the results achieved by SMDI. The results have shown that noise can seriously impact the measured accuracy of resistive sensors by SMDI and, differently from the ADC measurements, the accuracy cannot be improved by averaging on multiple measurements. A mitigation strategy to estimate the noise level and to improve the measurement accuracy of resistive sensors by SMDI was also proposed.

Keywords: resistive sensors; microcontrollers; ADC; simulations; sensor direct interface; noise; GPIO

Academic Editor(s): Name

Published: date

Citation: Grossi, M.; Omaña, M. Impact of Electrical Noise on the Accuracy of Resistive Sensor Measurements Using Sensor-to-Microcontroller Direct Interface. *Eng. Proc.* **2025**, *volume number*, x. https://doi.org/10.3390/xxxxx

1. Introduction

Sensors are devices capable of accurately measuring different types of quantities and are normally used in different types of applications, such as environmental monitoring [1–4], food quality and safety analysis [5–10], structural health monitoring of civil infrastructures [11–14], microbial contamination detection [15–19], and industry 4.0

applications [20–23]. In particular, the integration of low-power computing devices, sensors, and wireless communication technologies has led to the development of wireless sensor networks (WSNs), where large amount of data are acquired and shared with other sensor nodes and servers in the cloud [24–27]. Sensor data are normally acquired by microcontrollers or Field Programmable Gate Arrays (FPGAs) using analog-to-digital converters (ADCs), either integrated in the computing device or external [28–31].

WSNs are usually powered by batteries and/or energy harvesting devices, thus the sensor node power consumption is of paramount importance [32–34]. From this point of view, sensor-to-microcontroller direct interface (SMDI) is a technique that can be used to acquire sensor data without the use of an ADC, thus providing significant advantages in terms of low power consumption [35,36]. SMDI exploits the Schmitt triggers integrated in the general purpose input output (GPIO) interface of microcontrollers and FPGAs to directly interface the sensors analog output signal with the digital input pins of the computing device. SMDI has been exploited for the measurement of different types of sensors, such as resistive sensors [37–40], capacitive sensors [41–44], inductive sensors [45–47], as well as sensors featuring an output voltage signal [48].

As known, noise affects the reliability of electronic systems and can produce a severe limitation of the system reliability [49,50]. In particular, in the case of sensors, the noise contributes to the decrease of the signal-to-noise ratio and the measurement accuracy. Thus, we have investigated the impact of the noise on the measurement accuracy of resistive sensors using the SMDI technique. Different types of electrical noise can impact the reliability of electronic circuits, and they are typically classified in two different groups: intrinsic (or internal) noise and external noise [51]. Intrinsic noise refers to all the noise types that are generated inside an electronic device, such as thermal noise (produced by the random thermal agitation of electrons and holes in a conductor), shot noise (produced by the random arrival of electrons and holes at a discontinuous interface inside a device), flicker noise (that is usually found in transistors operating at low frequency), and transit time noise (produced by the energy transfer between electrons and ions). External noise, instead, refers to all types of noise that are generated outside of electronic devices, such as crosstalk noise and electromagnetic noise. Another classification for noise types is related to the shape of their power spectral density (PSD), as a function of frequency (f). White noise presents a flat PSD, while pink noise features a PSD proportional to f^{-1}, red noise features a PSD proportional to f^{-2}, blue noise features a PSD proportional to f, and violet noise features a PSD proportional to f^2. Our study considers only white noise as electrical noise source. The study was carried out by electrical level simulations with LTSpice [51] (with validation on preliminary experimental measurements), using a set of standard resistors of value between 100 Ω and 10 kΩ to represent a realistic working range for the values of a resistive sensor, and comparing the results with the case of measurements carried out using a 12-bit ADC for reference. The results have shown that measurements carried out using SMDI are strongly affected by noise and different noise types (gaussian white noise or uniform white noise) can have a different impact on the measurement accuracy. Moreover, the presence of noise can seriously degrade the measurement accuracy also in the case the measured sensor value is averaged on a large number of samples. In order to address these issues, we have proposed a mitigation strategy that can compensate the impact of noise on the measurement accuracy. It is based on the idea to use a programmable potentiometer in order to compensate the impact of noise by performing periodic calibrations on its value.

The paper is structured as follows. In Section 2, the simulation setups for the resistive sensor measurements using the SMDI technique and the 12-bit ADC are presented. In Section 3, the simulation results are presented and the accuracy achieved with the SMDI-based measurements and the ADC-based measurements are compared. In Section 4, the simulation results are discussed and a mitigation strategy to improve the measurement accuracy for the SMDI technique is presented. In Section 5, the simulations results are validated by experimental measurements on a microcontroller. Finally, conclusions are presented in Section 6.

2. Simulation Setup

The study has been carried out by electrical level simulations with LTSpice [52], considering a 180 nm CMOS technology. In Section 2.1, the simulation setup for the case of SMDI-based measurements is presented, while in Section 2.2, the simulation setup for the case of ADC-based measurements is presented.

2.1. SMDI-Based Measurements

Sensor-to-microcontroller direct interface (SMDI) is a technique that can be used to acquire sensor data without the use of an ADC, by interfacing the sensor directly to digital input-output pins of a microcontroller. The simulation setup for a resistive sensor R_T, measured with a microcontroller using the SMDI technique, is shown in Figure 1, where C is a discrete external capacitance.

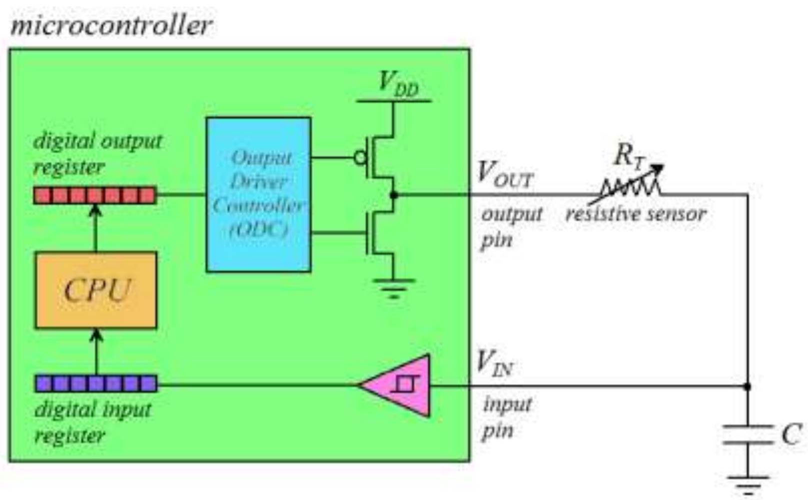

Figure 1. Simulation setup for a resistive sensor R_T measured using the SMDI technique.

SMDI exploits the Schmitt triggers integrated in the GPIO interface of microcontrollers to create an astable oscillator (with time constant R_TC) whose period is measured, using the digital timers integrated in the microcontroller, to estimate the resistive sensor value R_T. The analog voltage V_{IN} on an input pin of the microcontroller is fed to the non-inverting Schmitt trigger integrated in the GPIO interface of the microcontroller. The Schmitt trigger features two threshold voltages (V_H and V_L) so that, if $V_{IN} > V_H$ then the Schmitt trigger output is V_{DD}, while if $V_{IN} < V_L$ then the Schmitt trigger output is 0 V.

The microcontroller CPU acquires the digital value at the Schmitt trigger output and controls the Output Driver Controller (ODC) module so that the voltage at the output pin (V_{OUT}) is the complement of the Schmitt trigger output value.

The working principle of the measurement of R_T using SMDI can be defined as follows. Initially, it is $V_{IN} = V_L$, $V_{OUT} = V_{DD}$, and the capacitance C is charged with time constant R_TC (i.e., V_{IN} increases). When it is $V_{IN} = V_H$, the Schmitt trigger output switches from 0 V to V_{DD} and V_{OUT} switches from V_{DD} to 0 V. Then, the charging step of the capacitance (whose duration is indicated with t_H) terminates and the discharging of the capacitance C starts. When it is $V_{IN} = V_L$, the Schmitt trigger output switches from V_{DD} to 0 V and V_{OUT} switches from 0 V to V_{DD}. Then, the discharging step of the capacitance (whose duration is indicated with t_L) terminates and the charging of the capacitance C starts again. The values of t_H and t_L can be expressed as [40]:

$$t_H = R_T C \int_{V_L}^{V_H} \frac{1}{V_{DD} - V_{IN}} dV_{IN} = R_T C \cdot log \frac{V_{DD} - V_L}{V_{DD} - V_H} \tag{1}$$

$$t_L = -R_T C \int_{V_H}^{V_L} \frac{1}{V_{IN}} dV_{IN} = R_T C \cdot log \frac{V_H}{V_L} \tag{2}$$

The oscillation period T_P of the signals V_{IN} and V_{OUT} can be measured using the digital timers integrated in the microcontroller and can be expressed as:

$$T_P = t_H + t_L = R_T C \cdot log \frac{V_H(V_{DD} - V_L)}{V_L(V_{DD} - V_H)} \tag{3}$$

and the value of the resistive sensor can be calculated as:

$$R_T = \frac{T_P}{C \cdot log \frac{V_H(V_{DD} - V_L)}{V_L(V_{DD} - V_H)}} \tag{4}$$

The simulation setup of Figure 1 was implemented in LTSpice by using an ideal non inverting Schmitt trigger with threshold voltages of V_H = 1.9 V and V_L = 1.4 V, a power supply of V_{DD} = 3.3 V, a value for the capacitance C of 100nF, seven different values for the resistive sensor R_T (100 Ω, 250 Ω, 500 Ω, 1000 Ω, 2500 Ω, 5000 Ω, 10,000 Ω). The choice of fixed Schmitt trigger thresholds (V_H = 1.9 V and V_L = 1.4 V) has been considered as a case study. As discussed in [48], these thresholds can present significant different values for different devices. Moreover, slight differences in the Schmitt trigger thresholds for a single device also occur due to parameters dispersion introduced during manufacturing. Thus, to make accurate estimations of the sensor value, the exact values of the Schmitt trigger thresholds must be determined before the measurements. The operations performed by the microcontroller CPU were emulated by connecting a NOT digital gate between the output of the Schmitt trigger and the microcontroller output pin. The impact of the noise on the sensor measurement accuracy was evaluated by placing a white noise voltage generator (uniformly distributed) in series with the input pin of Figure 1. Nine different values of the white noise peak-to-peak voltage were evaluated (1.25 mV, 2.5 mV, 5 mV, 10 mV, 20 mV, 33.3 mV, 40 mV, 50 mV, 100 mV).

2.2. ADC-Based Measurements

The standard technique for sensors measurement by a microcontroller is based on the use of an ADC (integrated in the microcontroller or external) to acquire the analog information from the sensor and translate it to a digital format for data processing. In the case of a resistive sensor, a typical measurement setup is presented in Figure 2.

The measurement setup shown in Figure 2 exploits a Wheatstone bridge to generate a differential voltage ($V_{IN+} - V_{IN-}$) that is used to estimate the resistive sensor value R_T. Indicated with R_{REF} a reference resistor of known value, it is:

$$V_{IN+} = \frac{R_T}{R_T + R_{REF}} V_{DD} \tag{5}$$

Since it is $V_{IN-} = V_{DD}/2$, then it is:

$$V_{IN+} - V_{IN-} = \frac{V_{DD}}{2} \frac{R_T - R_{REF}}{R_T + R_{REF}} \tag{6}$$

The differential voltage $V_{IN+} - V_{IN-}$ is sampled and quantized by the ADC and a digital word $D_{11}D_{10} \ldots D_1D_0$ is generated and fed to the microcontroller for data processing.

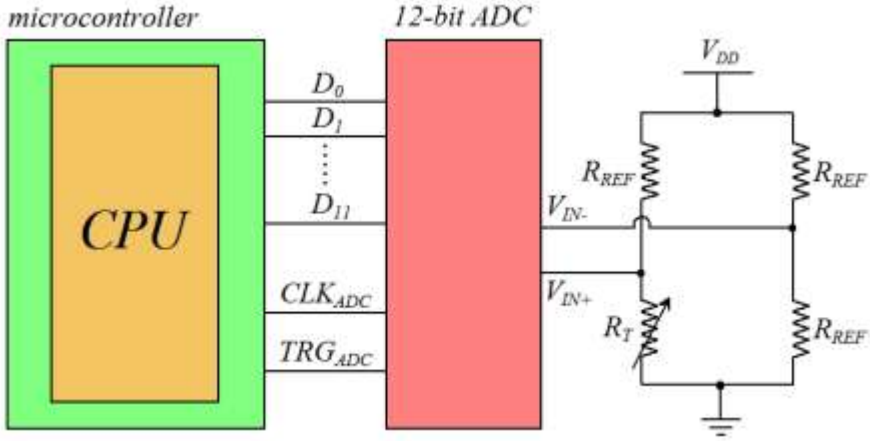

Figure 2. Simulation setup for a resistive sensor R_T measured using a 12-bit ADC.

The simulation setup shown in Figure 2 has been implemented in LTSpice considering a 12-bit differential input ADC (LTC2311-12) [53], a power supply of V_{DD} = 3.3 V, a value for the reference resistor R_{REF} of 1 kΩ, seven different values for the resistive sensor R_T (100 Ω, 250 Ω, 500 Ω, 1000 Ω, 2500 Ω, 5000 Ω, 10,000 Ω). The impact of the electrical noise on the sensor measurement accuracy has been evaluated by placing a white noise voltage generator (uniformly distributed) between the node V_{IN+} and the non-inverting input of the ADC in Figure 2. Nine different values of the white noise peak-to-peak voltage were evaluated (1.25 mV, 2.5 mV, 5 mV, 10 mV, 20 mV, 33.3 mV, 40 mV, 50 mV, 100 mV). The characteristic of the 12-bit ADC output as function of the resistive sensor value R_T in the case of noise-free operating condition is presented in Figure 3, where $V_{OUT,ADC}$ represents the analog equivalent of the ADC digital output $D_{11}D_{10} \ldots D_1D_0$. As can be seen, the characteristic is quasi-linear, with deviations from the linear behavior when the sensor resistance R_T deviates from the reference resistance R_{REF} of about one order of magnitude.

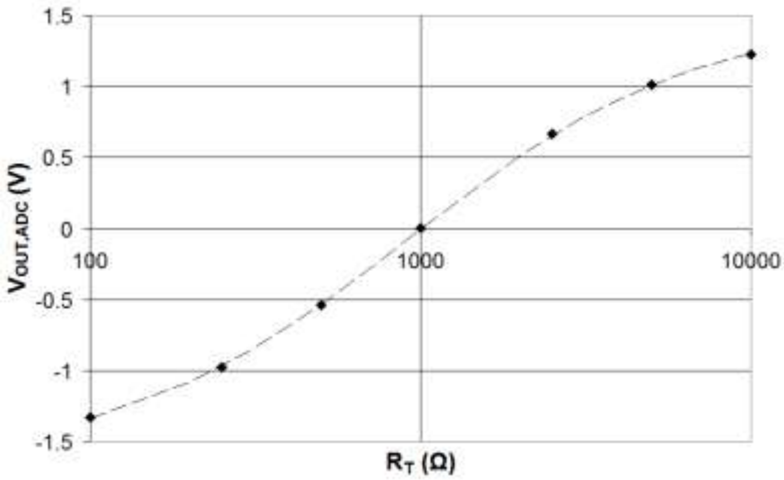

Figure 3. Characteristic of the 12-bit ADC output as function of R_T.

3. Simulation Results

The accuracy achieved in the case of a resistive sensor R_T has been evaluated for both the SMDI-based measurements and the ADC-based measurements according to the operative conditions described in Section 2.1 and Section 2.2, respectively. The measured R_T

has been evaluated in terms of average value and standard deviation, by carrying out 100 simulations for each operative condition. The simulation results for the case of the SMDI-based measurements are reported in Section 3.1, while the simulations results for the case of the ADC-based measurements are reported in Section 3.2.

3.1. SMDI-Based Measurements

The average value of the measured resistive sensor R_T is plotted in Figure 4 as function of the peak-to-peak voltage noise ($V_{noise,PP}$), for the case of a sensor resistance of nominal value 5 kΩ. As can be seen, the average value of measured R_T decreases linearly with the increase of $V_{noise,PP}$ and deviates from its nominal value as $V_{noise,PP}$ increases.

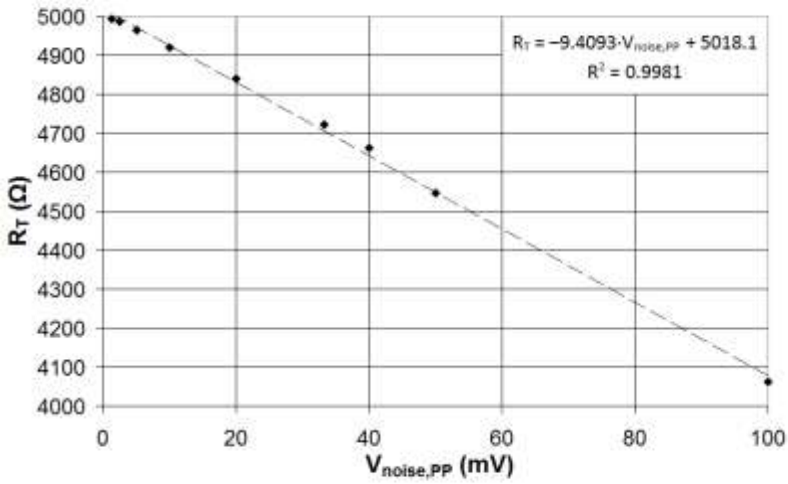

Figure 4. Average value of the measured R_T as function of the peak-to-peak voltage noise in the case of a sensor of nominal value 5 kΩ.

The measured values of R_T are presented in Table 1, in terms of average value (μ) and standard deviation (σ), as function of the nominal value of the sensor resistance and the peak-to-peak voltage noise.

Table 1. Measured values of R_T (average value and standard deviation) using the sensor-to-microcontroller direct interface technique in the case of different nominal values for the sensor resistance and for different values of the noise level.

	R_T (Ω)													
	100		**250**		**500**		**1000**		**2500**		**5000**		**10,000**	
$V_{noise,PP}$ (mV)	**μ**	**σ**	**μ**	**σ**	**μ**	**σ**	**μ**	**σ**	**μ**	**σ**	**μ**	**σ**	**μ**	**σ**
1.25	101.00	0.08	251.04	0.21	500.89	0.35	1000.5	0.64	2498.4	1.04	4993.6	1.66	9984.5	3.65
2.5	100.99	0.16	250.88	0.38	500.49	0.56	999.01	1.03	2494.2	1.78	4985.6	3.39	9965.6	5.31
5	100.91	0.27	250.68	0.61	498.84	0.87	996.33	1.70	2484.4	3.10	4963.8	4.47	9925.4	7.05
10	100.68	0.49	249.12	0.93	496.43	1.48	989.59	2.72	2465.9	4.39	4919.6	7.79	9835.8	12.9
20	99.41	0.73	246.09	1.54	488.47	2.01	971.34	3.28	2417.0	7.08	4840.7	10.8	9644.9	19.6
33.3	97.95	0.89	242.02	2.33	476.36	2.38	950.23	6.57	2366.3	11.9	4723.0	20.0	9416.5	32.7
40	97.18	1.18	237.50	2.14	472.03	3.92	941.65	5.42	2331.8	13.3	4661.1	18.4	9302.2	24.9
50	95.99	1.70	234.42	3.09	464.78	4.35	925.23	7.40	2286.8	16.4	4546.8	18.5	9100.2	34.1
100	88.49	2.67	214.40	4.68	424.73	6.46	841.96	8.53	2064.6	29.0	4062.7	19.5	8154.9	46.5

As can be seen, as $V_{noise,PP}$ increases, the average value of the measured R_T decreases and deviates from its nominal value, while the standard deviation increases. Thus, in the case of high levels of noise, even if the measured value of R_T is averaged on a large number of measurements, a good level of accuracy cannot be achieved.

The relative error (in percent) of the measured resistance R_T is evaluated using the parameter Δ_{ERROR}, that is defined by:

$$\Delta_{ERROR} = 100 \cdot \left|\frac{R_{T,meas} - R_T}{R_T}\right| \quad (7)$$

where $R_{T,meas}$ is the measured value of the sensor while R_T is its nominal value.

The obtained values of Δ_{ERROR} are presented as function of the nominal value of R_T in Figure 5 for the case of the minimum level of electrical noise ($V_{noise,PP}$ = 1.25mV), and in Figure 6 for the case of the maximum level of noise ($V_{noise,PP}$ = 100 mV).

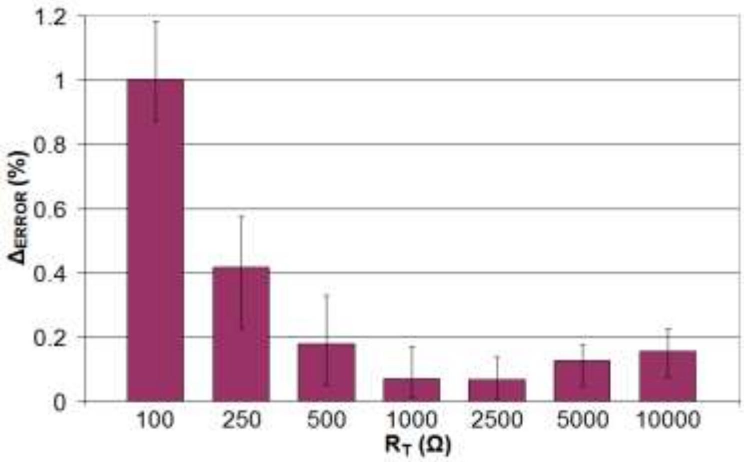

Figure 5. Measured Δ_{ERROR} as function of the nominal value of R_T for SMDI-based measurements in the case of the minimum level of noise ($V_{noise,PP}$ = 1.25 mV).

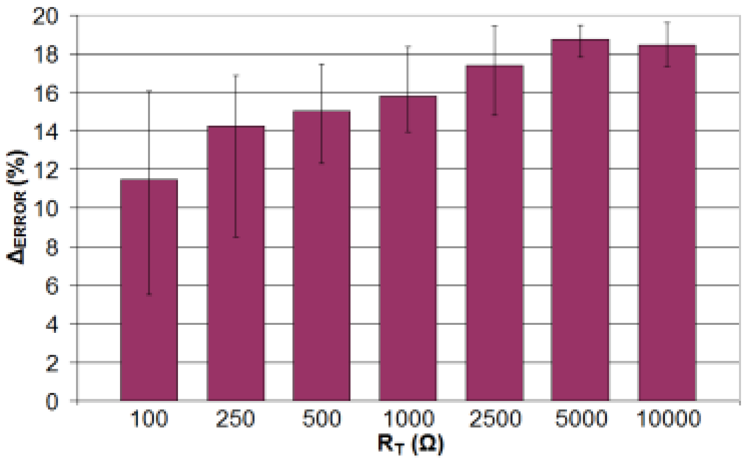

Figure 6. Measured Δ_{ERROR} as function of the nominal value of R_T for SMDI-based measurements in the case of the maximum level of noise ($V_{noise,PP}$ = 100 mV).

Data presented in Figures 5 and 6 confirms the results of Table 1. In the case of low levels of noise ($V_{noise,PP}$ = 1.25 mV), the SMDI technique achieves a very good accuracy with a relative error always lower than 1%, and even lower than 0.2% for values of R_T of 500 Ω or higher. In the case of high levels of noise ($V_{noise,PP}$ = 100 mV), instead, the achieved relative error is always very high (>10%).

3.2. ADC-Based Measurements

The measured values of R_T are presented in Table 2, in terms of average value (μ) and standard deviation (σ), as function of the nominal value of the sensor resistance and the peak-to-peak voltage noise. As can be seen, similarly to the case of SMDI-based measurements, the measured R_T standard deviation increases with the level of noise. However, differently from SMDI-based measurements, the average value of the measured R_T is almost independent of the noise level. Thus, in the case of ADC-based measurements, accurate values of the resistive sensor value can be achieved also in a noisy environment, if R_T is calculated by averaging on a large number of measurements.

Table 2. Measured values of R_T (average value and standard deviation) using the 12-bit ADC LTC2311-12 in the case of different values for the sensor resistance and for different values of the noise level.

	R_T (Ω)													
	100		**250**		**500**		**1000**		**2500**		**5000**		**10,000**	
$V_{noise,PP}$ (mV)	**μ**	**σ**	**μ**	**σ**	**μ**	**σ**	**μ**	**σ**	**μ**	**σ**	**μ**	**σ**	**μ**	**σ**
1.25	102.48	0.16	247.91	0.10	495.26	0.19	1003.0	0.64	2534.9	1.82	5025.3	4.41	9739.9	20.2
2.5	102.45	0.22	247.86	0.28	495.32	0.35	1003.0	0.64	2535.3	1.96	5027.2	5.94	9742.2	27.8
5	102.43	0.41	247.84	0.47	495.31	0.61	1003.0	1.02	2535.5	3.07	5027.2	9.16	9741.3	34.3
10	102.40	0.83	247.79	0.91	495.23	1.19	1002.9	1.91	2535.3	5.55	5026.7	16.0	9740.2	52.5
20	102.31	1.62	247.70	1.82	495.18	2.31	1002.8	3.83	2534.8	10.9	5026.2	30.8	9737.0	98.6
33.3	102.16	2.76	247.55	3.06	495.05	3.84	1002.7	6.32	2534.5	17.9	5025.7	50.8	9737.0	159
40	102.10	3.31	247.52	3.70	495.01	4.62	1002.5	7.59	2534.3	21.4	5025.5	60.4	9734.5	190
50	102.01	4.14	247.44	4.63	494.89	5.79	1002.5	9.42	2534.1	26.4	5024.8	74.9	9732.8	236
100	101.61	8.28	247.03	9.23	494.55	11.6	1002.1	18.9	2533.3	53.5	5022.5	152	9740.8	470

The values of the relative error (Δ_{ERROR}), as defined in Equation (7), are presented as function of the nominal value of R_T in Figure 7 for the case of the minimum level of noise ($V_{noise,PP}$ = 1.25 mV) and in Figure 8 for the case of the maximum level of noise ($V_{noise,PP}$ = 100mV).

As can be seen, in the case of low levels of noise ($V_{noise,PP}$ = 1.25 mV), measurements carried out by the SMDI technique are more accurate (average Δ_{ERROR} of 0.28%) than the ADC-based measurements (average Δ_{ERROR} of 1.29%). On the contrary, in the case of high levels of noise ($V_{noise,PP}$ = 100 mV), measurements carried out by the SMDI technique are less accurate (average Δ_{ERROR} of 15.88%) than the ADC-based measurements (average Δ_{ERROR} of 3.27%).

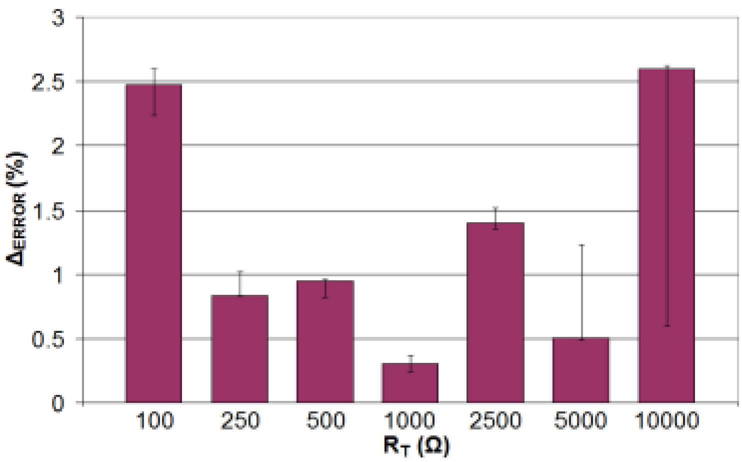

Figure 7. Measured Δ_{ERROR} as function of the nominal value of R_T for ADC-based measurements in the case of the minimum level of noise ($V_{noise,PP}$ = 1.25 mV).

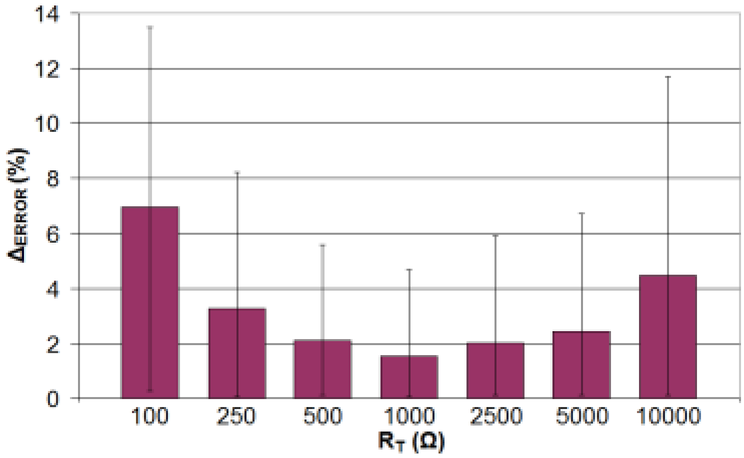

Figure 8. Measured Δ_{ERROR} as function of the nominal value of R_T for ADC-based measurements in the case of the maximum level of noise ($V_{noise,PP}$ = 100 mV).

4. Discussion

The results presented in Section 3 have shown that, as expected, higher levels of noise degrade the accuracy of sensor measurements, both in the case of ADC-based measurements and SMDI-based measurements. In the case of ADC-based measurements, however, the average value of sensor data is almost unaffected by the level of noise, thus an higher measurement accuracy can be achieved by averaging on a large number of samples. This is not the case for SMDI-based measurements, where the average value of the sensor resistance deviates from its nominal value as the noise level increases, thus preventing the possibility to improve the measurement accuracy by averaging on multiple samples. In this section, the reasons for the strong impact of noise on the accuracy of SMDI-based measurements are investigated, and a possible mitigation strategy to improve the accuracy of SMDI-based measurements in a noisy environment will be presented.

The waveforms of the voltage signals acquired during a simulation of the resistive sensor measurement with SMDI are presented in Figure 9. With reference to Figure 1, the voltage V_{IN} (input of the Schmitt trigger integrated in the microcontroller GPIO interface) is presented in the case of a signal with high electrical noise level (100 mV peak-to-peak amplitude) as well as in the case of the noise free signal.

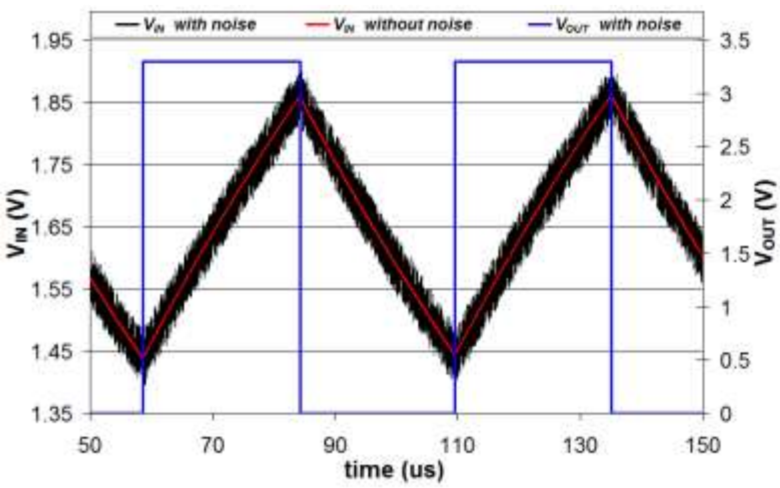

Figure 9. Waveforms of the voltage signals acquired during a simulation of the resistive sensor measurement using SMDI, in presence and absence of noise.

As can be seen, the presence of the noise results in the triggering of the Schmitt trigger thresholds (V_H and V_L) before the noise free voltage signal reaches these thresholds. This results in an increase of the detected V_L and a decrease of the detected V_H, and thus in a decrease of the measured period T_P as defined by Equation (3). Then, in accordance with Equation (4), this results in a decrease of the measured sensor resistance R_T, as also shown in the results of Section 3.1 (Figure 4 and Table 1). Moreover, the impact of the noise on the measurement accuracy is higher in the case of slower variations of the signal V_{IN}, thus in the case of higher nominal values of R_T, as also shown in Figure 6.

To investigate how different types of noise impact on the accuracy of SMDI-based measurements, we have evaluated the detected average values of the Schmitt trigger thresholds (V_L and V_H) during a SMDI measurement under different levels of electrical noise, for R_T = 10kΩ, and two different types of noise: uniformly distributed white noise signal and Gaussian distributed white noise signal. The results are shown as function of the noise standard deviation (σ_{noise}) in Figure 10 for the voltage threshold V_L and in Figure 11 for the voltage threshold V_H, with the average values of V_L and V_H calculated by averaging on 1000 measurements. As expected, the threshold voltage V_L increases with noise level, while the threshold voltage V_H decreases with noise level. Moreover, the amount of deviation of the detected Schmitt trigger threshold voltages from their nominal value changes for different types of noise: the deviation is stronger for a Gaussian distributed white noise than for a uniformly distributed white noise.

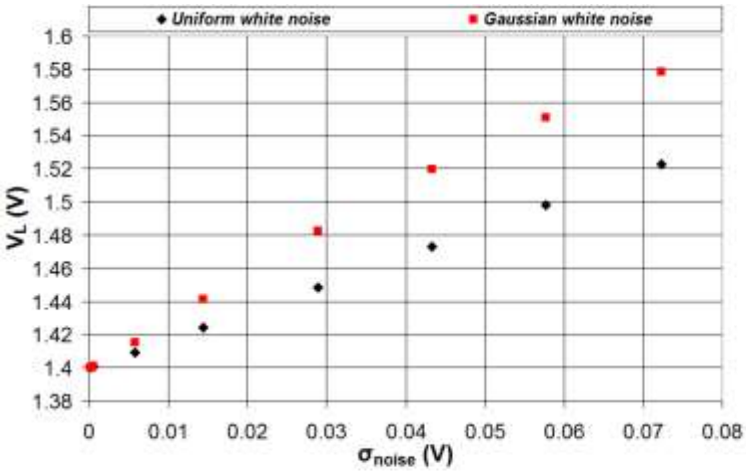

Figure 10. Average value of the detected Schmitt trigger threshold V_L as function of the noise level.

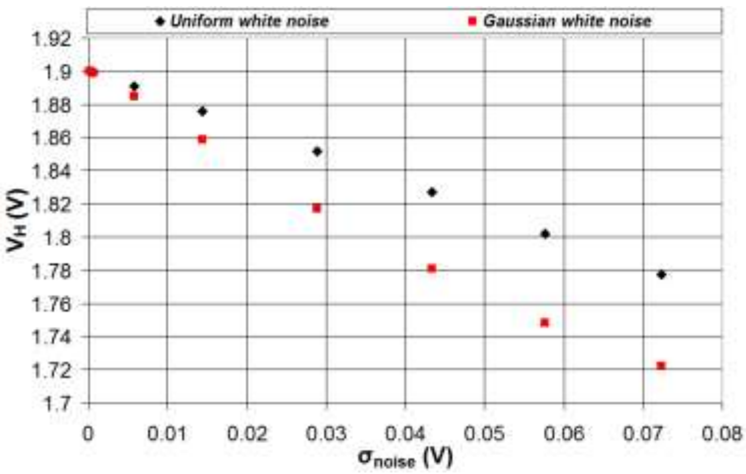

Figure 11. Average value of the detected Schmitt trigger threshold V_H as function of the noise level.

Based on the obtained results, in order to achieve an acceptable measurement accuracy, it is of paramount importance to design a strategy to mitigate the impact of the noise for resistive sensor measurements carried out by the SMDI technique. A possible solution is to replace the standard SMDI measurement setup presented in Figure 1 with the proposed measurement setup shown in Figure 12.

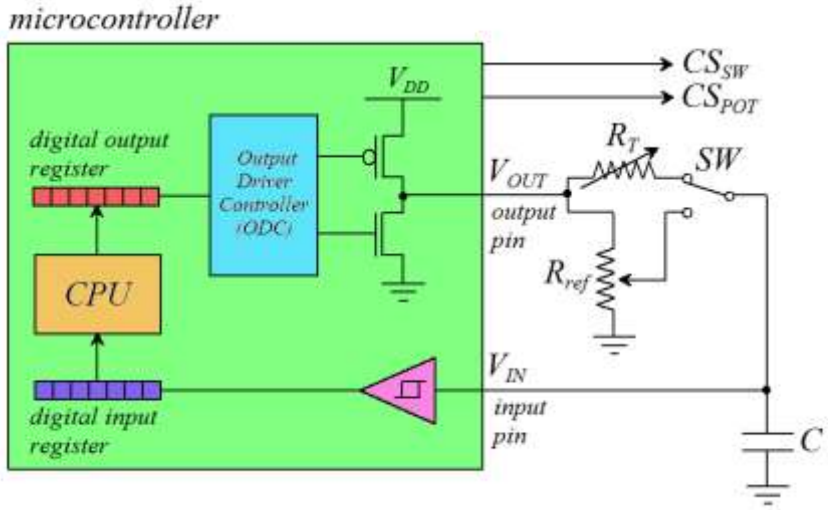

Figure 12. Proposed measurement setup to mitigate the impact of noise in SMDI-based measurements of resistive sensors.

The resistor R_T in Figure 12, represents the resistive sensor under test, while R_{ref} is a digital potentiometer, and SW is an analog switch controlled by the microcontroller digital output pins (CS_{SW} and CS_{POT}). In normal operating conditions, the switch SW connects the resistive sensor R_T between the microcontroller input and output pins, and the sensor value is measured using the procedure described in Section 2.1. The sensor value (R_T) is calculated by comparing the measured period (T_P) with a set of reference values determined during a calibration procedure and stored in a look-up table.

The calibration procedure is carried out at regular time intervals to guarantee that all the measurements carried out after the calibration experience the same noise level as during the calibration.

During the calibration procedure, the switch SW is set to disconnect the sensor R_T and connect the digital potentiometer R_{ref} between the microcontroller input and output pins. At this point, the period T_P defined in Equation (2) is measured (by averaging on an adequate number of measurements) for each value of the digital potentiometer R_{ref} (between 0 Ω and the digital potentiometer full scale resistance with step ΔR_{ref}). The look-up table presenting the measured resistance value for the different values of the measured period is stored in the microcontroller memory. During the normal operating conditions, this look-up table is used to estimate the sensor resistance from the measured period T_P. More accurate estimation of the sensor resistance R_T is possible by using a digital potentiometer with higher resolution (i.e., lower ΔR_{ref}) but at the cost of higher memory occupation to store the calibration look-up table.

Simulations have been carried out to evaluate the maximum error in R_T estimation as function of the digital potentiometer resolution. The simulations have been performed for the case of uniform white noise with 40 mV peak-to-peak voltage. Both the sensor R_T (during the normal operating conditions) and the potentiometer R_{ref} (during the calibration procedure) are determined by averaging 50 measurements. A dataset of 50 different R_T

values was generated with a uniform probability distribution between 100 Ω and 10 kΩ. The simulation results have shown that the sensor relative error (Δ_{ERROR} as defined in Equation (7)) decreases, as expected, by increasing the digital potentiometer resolution (i.e., decreasing ΔR_{ref}): we obtained a value of Δ_{ERROR} of 2.49% for ΔR_{ref} = 25 Ω, a value of Δ_{ERROR} of 2.02% for ΔR_{ref} = 20 Ω, a value of Δ_{ERROR} of 1.25% for ΔR_{ref} = 12.5 Ω, a value of Δ_{ERROR} of 0.85% for ΔR_{ref} = 10 Ω, and a value of Δ_{ERROR} of 0.46% for ΔR_{ref} = 3.33 Ω. Decreasing ΔR_{ref} below 3.33 Ω does not produce any improvement in the measurement accuracy.

5. Experimental Measurements on a Microcontroller

In this section, the simulation results presented in the previous sections are validated by experimental measurements carried out on a low-cost microcontroller.

The measurement setup is shown in Figure 13. It consists of a Nucleo-L152RE development board that integrates a STM32L152RET6 microcontroller (ST Microelectronics, Geneva, Switzerland) and a laptop PC that is used to communicate with the microcontroller board using the USB-UART interface.

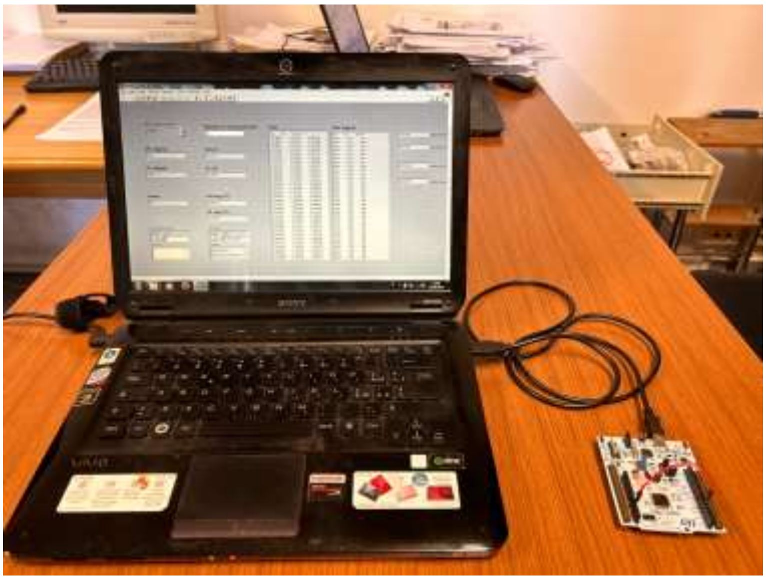

Figure 13. Experimental measurement setup to estimate the Schmitt trigger threshold voltages under different noise levels.

The threshold voltages (V_H and V_L) of the Schmitt trigger integrated in an input pin of the microcontroller have been measured (using the integrated 12-bit DAC) under different noise levels, with the following procedure.

1. The output of the microcontroller DAC is shorted with the input pin to be tested using a cable. Cables of three different lengths (11.5 cm, 26.5 cm, and 102.5 cm) were tested, since the longer the cable, the higher the probability that electromagnetic interference degrades the signal-to-noise ratio.
2. Meanwhile, the microcontroller generates an analog voltage at the DAC output that increases from 0 V to 3.3 V, with steps of 12.89 mV. After the DAC output voltage is increased to e new value, the microcontroller waits 2 ms to allow the voltage stabilization, and then reads the value of the digital input pin. The Schmitt trigger threshold V_H is estimated as the DAC output voltage for which the input pin logic value switches from 0 to 1.
3. Then, the microcontroller generates an analog voltage at the DAC output that decreases from 3.3 V to 0 V, with steps of 12.89 mV. Again, after the DAC output voltage is decreased to a new value, the microcontroller waits 2 ms to allow the voltage

stabilization, and then reads the value of the digital input pin. The Schmitt trigger threshold V_L is estimated as the DAC output voltage for which the input pin logic value switches from 1 to 0.

The values of V_H and V_L have been measured 100 times and the measured values (average value and standard deviation) are reported in Figure 14 (for V_H) and in Figure 15 (for V_L) as function of the cable length.

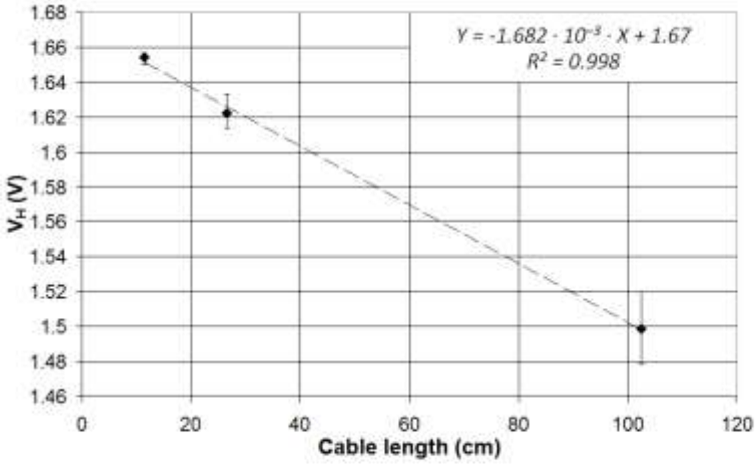

Figure 14. Measured values of the Schmitt trigger threshold voltage V_H as function of the cable length.

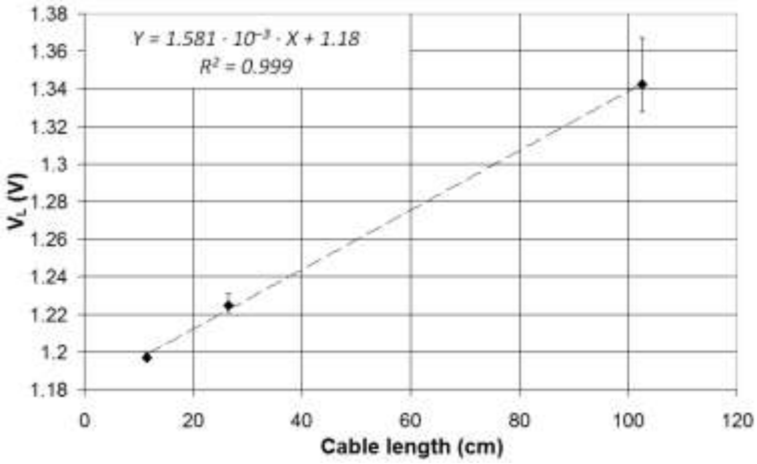

Figure 15. Measured values of the Schmitt trigger threshold voltage V_L as function of the cable length.

As can be seen, the measured Schmitt trigger threshold voltage V_H (V_L) decreases (increases) linearly (high determination coefficient, $R^2 > 0.998$) with the cable length, and thus with the electrical noise level. These experimental measurements confirm the simulation results, where the estimated Schmitt trigger threshold voltages change linearly with the standard deviation of the white noise signal (Figures 10 and 11).

6. Conclusions

In this paper, it was evaluated the impact of noise on the accuracy of resistive sensor measurements carried out by the sensor-to-microcontroller direct interface (SMDI) technique. The study was carried out by electrical level simulations with the software LTSpice and preliminary experimental measurements. The measurement accuracy of a resistive sensor was evaluated under different levels of white noise both in the case of SMDI-based measurements and ADC-based measurements. The simulation results have shown that, while in the case of ADC-based measurements the impact of the noise can be mitigated by averaging on a large number of measurements, in the case of SMDI-based measurements this solution is ineffective. Thus, a mitigation strategy was proposed to allow accurate measurements of resistive sensors using the SMDI technique in a noisy environment.

Author Contributions: Conceptualization, M.G.; methodology, M.G.; software, M.G.; validation, M.G.; formal analysis, M.G.; investigation, M.G.; resources, M.G.; data curation, M.G.; writing—original draft preparation, M.G.; writing—review and editing, M.G. and M.O.; visualization, M.G. and M.O.; supervision, M.G. and M.O.; project administration, M.G. and M.O. All authors have read and agreed to the published version of the manuscript.

Funding: This research received no external funding.

Institutional Review Board Statement: Not applicable.

Informed Consent Statement: Not applicable.

Data Availability Statement: Data sharing is not applicable to this article.

Conflicts of Interest: The authors declare no conflict of interest.

References

1. Dhall, S.; Mehta, B.R.; Tyagi, A.K.; Sood, K. A review on environmental gas sensors: Materials and technologies. *Sens. Int.* **2021**, *2*, 100116.
2. Han, P.; Mei, H.; Liu, D.; Zeng, N.; Tang, X.; Wang, Y.; Pan, Y. Calibrations of low-cost air pollution monitoring sensors for CO, NO_2, O_3, and SO_2. *Sensors* **2021**, *21*, 256.
3. Gavrilaș, S.; Ursachi, C.Ș.; Perța-Crișan, S.; Munteanu, F.D. Recent trends in biosensors for environmental quality monitoring. *Sensors* **2022**, *22*, 1513.
4. Liang, L. Calibrating low-cost sensors for ambient air monitoring: Techniques, trends, and challenges. *Environ. Res.* **2021**, *197*, 111163.
5. Grossi, M.; Valli, E.; Bendini, A.; Gallina Toschi, T.; Riccò, B. A Portable Battery-Operated Sensor System for Simple and Rapid Assessment of Virgin Olive Oil Quality Grade. *Chemosensors* **2022**, *10*, 102.
6. Grossi, M.; Bendini, A.; Valli, E.; Gallina Toschi, T. Field-deployable determinations of peroxide index and total phenolic content in olive oil using a promising portable sensor system. *Sensors* **2023**, *23*, 5002.
7. Sohrabi, H.; Sani, P.S.; Orooji, Y.; Majidi, M.R.; Yoon, Y.; Khataee, A. MOF-based sensor platforms for rapid detection of pesticides to maintain food quality and safety. *Food Chem. Toxicol.* **2022**, *165*, 113176.
8. Lu, L.; Hu, Z.; Hu, X.; Li, D.; Tian, S. Electronic tongue and electronic nose for food quality and safety. *Food Res. Int.* **2022**, *162*, 112214.
9. Dodero, A.; Escher, A.; Bertucci, S.; Castellano, M.; Lova, P. Intelligent packaging for real-time monitoring of food-quality: Current and future developments. *Appl. Sci.* **2021**, *11*, 3532.
10. Grossi, M.; Valli, E.; Glicerina, V.T.; Rocculi, P.; Gallina Toschi, T.; Riccò, B. Optical determination of solid fat content in fats and oils: Effects of wavelength on estimated accuracy. *Eur. J. Lipid Sci. Technol.* **2022**, *124*, 2100071.
11. Kaartinen, E.; Dunphy, K.; Sadhu, A. LiDAR-based structural health monitoring: Applications in civil infrastructure systems. *Sensors* **2022**, *22*, 4610.
12. Mishra, M.; Lourenço, P.B.; Ramana, G.V. Structural health monitoring of civil engineering structures by using the internet of things: A review. *J. Build. Eng.* **2022**, *48*, 103954.
13. Jayawickrema, U.M.N.; Herath, H.M.C.M.; Hettiarachchi, N.K.; Sooriyaarachchi, H.P.; Epaarachchi, J.A. Fibre-optic sensor and deep learning-based structural health monitoring systems for civil structures: A review. *Measurement* **2022**, *199*, 111543.
14. Rossi, M.; Bournas, D. Structural health monitoring and management of cultural heritage structures: A state-of-the-art review. *Appl. Sci.* **2023**, *13*, 6450.
15. Grossi, M.; Parolin, C.; Vitali, B.; Riccò, B. Computer vision approach for the determination of microbial concentration and growth kinetics using a low cost sensor system. *Sensors* **2019**, *19*, 5367.

16. Grossi, M.; Parolin, C.; Vitali, B.; Riccò, B. A portable sensor system for bacterial concentration monitoring in metalworking fluids. *J. Sens. Sens. Syst.* **2018**, *7*, 349–357.
17. Canciu, A.; Tertis, M.; Hosu, O.; Cernat, A.; Cristea, C.; Graur, F. Modern analytical techniques for detection of bacteria in surface and wastewaters. *Sustainability* **2021**, *13*, 7229.
18. Spagnolo, S.; De La Franier, B.; Davoudian, K.; Hianik, T.; Thompson, M. Detection of *E. coli* bacteria in milk by an acoustic wave aptasensor with an anti-fouling coating. *Sensors* **2022**, *22*, 1853.
19. Nnachi, R.C.; Sui, N.; Ke, B.; Luo, Z.; Bhalla, N.; He, D.; Yang, Z. Biosensors for rapid detection of bacterial pathogens in water, food and environment. *Environ. Int.* **2022**, *166*, 107357.
20. Kanoun, O.; Khriji, S.; Naifar, S.; Bradai, S.; Bouattour, G.; Bouhamed, A.; El Houssaini, D.; Viehweger, C. Prospects of wireless energy-aware sensors for smart factories in the industry 4.0 era. *Electronics* **2021**, *10*, 2929.
21. Varshney, A.; Garg, N.; Nagla, K.S.; Nair, T.S.; Jaiswal, S.K.; Yadav, S.; Aswal, D.K. Challenges in sensors technology for industry 4.0 for futuristic metrological applications. *Mapan* **2021**, *36*, 215–226.
22. Majid, M.; Habib, S.; Javed, A.R.; Rizwan, M.; Srivastava, G.; Gadekallu, T.R.; Lin, J.C.W. Applications of wireless sensor networks and internet of things frameworks in the industry revolution 4.0: A systematic literature review. *Sensors* **2022**, *22*, 2087.
23. Soori, M.; Arezoo, B.; Dastres, R. Internet of things for smart factories in industry 4.0, a review. *Internet Things Cyber-Phys. Syst.* **2023**, *3*, 192–204.
24. Gulati, K.; Boddu, R.S.K.; Kapila, D.; Bangare, S.L.; Chandnani, N.; Saravanan, G. A review paper on wireless sensor network techniques in Internet of Things (IoT). *Mater. Today Proc.* **2022**, *51*, 161–165.
25. Stankovic, J.A. Wireless sensor networks. *Computer* **2008**, *41*, 92–95.
26. Khalil, N.; Abid, M.R.; Benhaddou, D.; Gerndt, M. Wireless sensors networks for Internet of Things. In Proceedings of the 2014 IEEE Ninth International Conference on Intelligent Sensors, Sensor Networks and Information Processing (ISSNIP), Singapore, 21–24 April 2014; pp. 1–6.
27. Kandris, D.; Nakas, C.; Vomvas, D.; Koulouras, G. Applications of wireless sensor networks: An up-to-date survey. *Appl. Syst. Innov.* **2020**, *3*, 14.
28. Chen, C.H.; He, T.; Zhang, Y.; Temes, G.C. Incremental analog-to-digital converters for high-resolution energy-efficient sensor interfaces. *IEEE J. Emerg. Sel. Top. Circuits Syst.* **2015**, *5*, 612–623.
29. Krasilenko, V.G.; Nikolskyy, A.I.; Lazarev, A.A. Multichannel serial-parallel analog-to-digital converters based on current mirrors for multi-sensor systems. *Opt. Syst. Des.* **2012**, *8550*, 598–609.
30. Schroeder, D. Adaptive low-power analog/digital converters for wireless sensor networks. In Proceedings of the Third International Workshop on Intelligent Solutions in Embedded Systems, Hamburg, Germany, 20–20 May 2005; pp. 70–78.
31. Huang, J.S.; Kuo, S.C.; Chen, C.H. A multistep multistage fifth-order incremental delta sigma analog-to-digital converter for sensor interfaces. *IEEE J. Solid-State Circuits* **2023**, *58*, 2733–2744.
32. Singh, J.; Kaur, R.; Singh, D. Energy harvesting in wireless sensor networks: A taxonomic survey. *Int. J. Energy Res.* **2021**, *45*, 118–140.
33. Hu, H.; Han, Y.; Yao, M.; Song, X. Trust based secure and energy efficient routing protocol for wireless sensor networks. *IEEE Access* **2021**, *10*, 10585–10596.
34. Bhushan, S.; Kumar, M.; Kumar, P.; Stephan, T.; Shankar, A.; Liu, P. FAJIT: A fuzzy-based data aggregation technique for energy efficiency in wireless sensor network. *Complex Intell. Syst.* **2021**, *7*, 997–1007.
35. Reverter, F. The art of directly interfacing sensors to microcontrollers. *J. Low Power Electron. Appl.* **2012**, *2*, 265–281.
36. Reverter, F. Power consumption in direct interface circuits. *IEEE Trans. Instrum. Meas.* **2012**, *62*, 503–509.
37. Reverter, F. A microcontroller-based interface circuit for three-wire connected resistive sensors. *IEEE Trans. Instrum. Meas.* **2022**, *71*, 2006704.
38. Reverter, F. A direct approach for interfacing four-wire resistive sensors to microcontrollers. *Meas. Sci. Technol.* **2022**, *34*, 037001.
39. Grossi, M.; Omaña, M. Accuracy of NTC Thermistor Measurements Using the Sensor to Microcontroller Direct Interface. *Eng. Proc.* **2024**, *82*, 12.
40. Grossi, M.; Omaña, M.; Metra, C. Impact of aging on temperature measurements performed using a resistive temperature sensor with sensor-to-microcontroller direct interface. *Microelectron. Reliab.* **2025**, *169*, 115729.
41. Czaja, Z. A measurement method for lossy capacitive relative humidity sensors based on a direct sensor-to-microcontroller interface circuit. *Measurement* **2021**, *170*, 108702.
42. Czaja, Z. A measurement method for capacitive sensors based on a versatile direct sensor-to-microcontroller interface circuit. *Measurement* **2020**, *155*, 107547.

43. Reverter, F.; Casas, Ò. Interfacing differential capacitive sensors to microcontrollers: A direct approach. *IEEE Trans. Instrum. Meas.* **2009**, *59*, 2763–2769.
44. Gaitán-Pitre, J.E.; Gasulla, M.; Pallas-Areny, R. Analysis of a direct interface circuit for capacitive sensors. *IEEE Trans. Instrum. Meas.* **2009**, *58*, 2931–2937.
45. Kokolanski, Z.; Jordana, J.; Gasulla, M.; Dimcev, V.; Reverter, F. Direct inductive sensor-to-microcontroller interface circuit. *Sens. Actuators A Phys.* **2015**, *224*, 185–191.
46. Kokolanski, Z.; Jordana, J.; Gasulla, M.; Dimcev, V.; Reverter, F. Microcontroller-based interface circuit for inductive sensors. *Procedia Eng.* **2014**, *87*, 1251–1254.
47. Asif, A.; Ali, A.; Abdin, M.Z.U. Resolution enhancement in directly interfaced system for inductive sensors. *IEEE Trans. Instrum. Meas.* **2018**, *68*, 4104–4111.
48. Grossi, M. Efficient and Accurate Analog Voltage Measurement Using a Direct Sensor-to-Digital Port Interface for Microcontrollers and Field-Programmable Gate Arrays. *Sensors* **2024**, *24*, 873.
49. Jones, B.K. Electrical noise as a reliability indicator in electronic devices and components. *IEE Proc.-Circuits Devices Syst.* **2002**, *149*, 13–22.
50. Demir, A.; Sangiovanni-Vincentelli, A. *Analysis and Simulation of Noise in Nonlinear Electronic Circuits and Systems*; Springer Science & Business Media: Berlin/Heidelberg, Germany, 2012; Volume 425.
51. Vasilescu, G. *Electronic Noise and Interfering Signals: Principles and Applications*; Springer Science & Business Media: Berlin/Heidelberg, Germany, 2006.
52. LTSpice Circuit Simulator. Available online: https://www.analog.com/en/resources/design-tools-and-calculators/ltspice-simulator.html (accessed on 15 May 2025).
53. LTC2311-12 ADC. Available online: https://www.analog.com/en/products/ltc2311-12.html (accessed on 15 May 2025).